III The Design of the Shower Maximum Detectors

III.1 Mechanical Design of the SMD

III.1.1 Introduction

Since the beginning of the STAR EMC project a variety of technologies were considered for use in the STAR Shower Maximum Detector (SMD). A detectors based on scintillation hodoscope with fiber readout "SciFi" gaseous wire/strip chambers "wire/strip", and plastic streamer tube "PST" were considered as a candidate for SMD at STAR. During 1992-1997 extensive tests and Monte Carlo calculations were carried out to evaluate the three candidate SMD media. Four different "SciFi", four "wire/strip" and "strip/strip" and one "PST" prototypes were designed, constructed and tested on electron and hadron beams at Protvino U-70 and Brookhaven AGS accelerators. The SMDs performances were studied at the energy range from 0.5 to 26.6 GeV, for a different detector positions inside the EMC and different detector granularities. The results of this investigations shows that both "SciFi" and proportional gaseous detector in "strip/strip" readout configuration were well-suited for the STAR where electromagnetic shower must be precisely localized in space and their characteristic transverse size parameters must be measured. An independent energy measurement near the shower maximum is also needed to improve the overall hadron discrimination power of the non-segmented EMC and SMD. In order to accomplish its measurement functionality goals, the EMC/SMD must measure photons and electrons, often in large hadronic backgrounds. An important component of our discrimination between electromagnetic and hadronic showers and our ability to discriminate photon pairs in a single tower will come from the characteristic transverse shower shape and dimensions at a point near the energy density maximum of an electromagnetic shower in the longitudinal direction. The observation direct photons, whether in p+p or Au+Au, will rely in an essential way on the ability to identify an isolate photons in this manner. Furthermore, the construction of an invariant mass for photon pairs or dielectrons, particularly at high Pt, requires precise localization of the showers. The combination of large EMC cell size and fine-grained detector(SMD) at a few radiation length deep is the most economical way to do the required electromagnetic shower localization and characterization. It has been shown that this approach allows direct photon physics with acceptable error bars (e.g. CDF).The final design consideration for the SMD detector involve compromises between the physics requirements, mechanical constraints, and cost. The SMD is designed as a wire/strip array consisting of a double layer of proportional gas counters which are read out using orthogonal sets of cathode strips (pads). The charge collected on the cathode pads provides information on the position of the anode avalanche and finally gives the information about the shower shape and energy deposition at depth 5X0 inside the EMC. Detailed simulation have been conducted to study the optimum depth to place the SMD detector within the EMC. A compromise is required by the very broad energy range of photons and electrons encountered in the entire STA physics program. A depth 5X0 has been found to provide the acceptable gamma/pi0 separation at the highest energies while providing good discrimination for the soft photons encountered in the heavy ion program and in asymmetric pi0 decay.

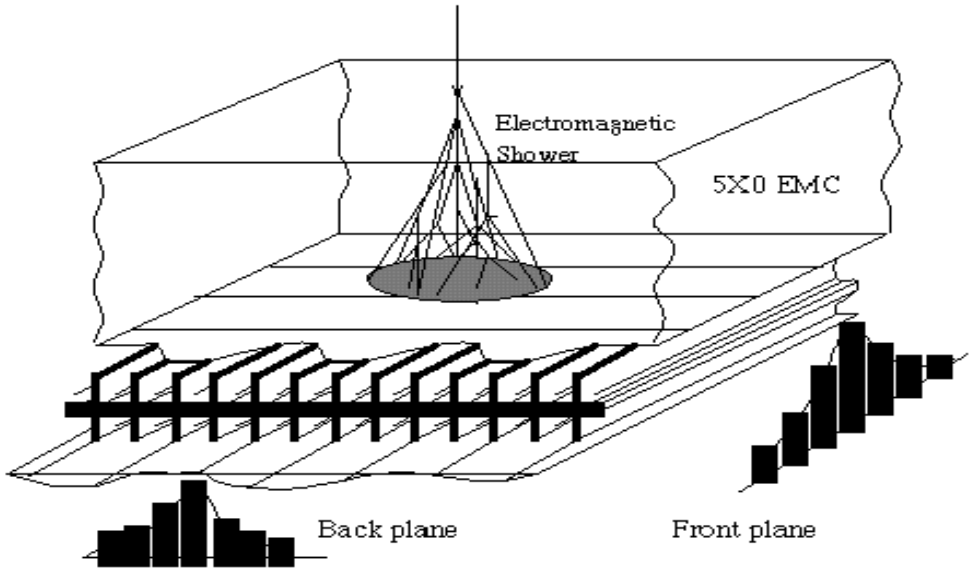

Figure III.1

III.1.2 Component Design, Fabrication and Quality Control

Careful Monte-Carlo studies at IHEP have led to the following table of parameters for the physical design of the SMD to achieve a reasonable fraction of the physics goals. The physics requirements were to achieve reasonably low occupancy in Au+Au collisions, segmentation comparable with the expected transverse size of the showers and good two-shower resolving power.

Mechanically, the SMD should have as little impact as possible on the performance of the EMC. This places difficult constraints on both the rigidity and flatness of the SMD modules, leading to a design which transports the strip signals to preamplifier electronics boards placed at the end of the modules, rather than embedding the electronics within the EMC. This decision also improves the modularity of the SMD design, enabling better access to the completed units.

SMD Design Parameters

Chamber Position inside EMC	5X0
Rapidity Coverage (Single Module)	$\Delta\eta = 1.0$
Azimuthal Coverage(Single Module)	$\Delta\phi = 0.105$ (6°)
Occupancy (p+p)	≈1%
Occupancy (Au+Au)	> 5 to ≈25% (depends on the threshold cut)
Chamber Depth (Cathode to Cathode)	20.6 mm
Anode Wire Diameter	50 μm
Gas Mixture	90%-Ar /10%-CO_2
Gas Amplification	≈3000
Signal Length	110 ns
Strip Width (Pitch) in η for $\|\eta\|<0.5$	1.46 (1.54) cm

Strip Width (Pitch) in η for $\|\eta\|>0.5$	1.88 (1.96) cm
Strip Width (Pitch) in ϕ	1.33 (1.49) cm
Number of Strips per Module	300
Total Number of Modules	120
Total Number of Readout Channels	36000

Table III.1.

III.1.3 Detector Assembly and Quality Control

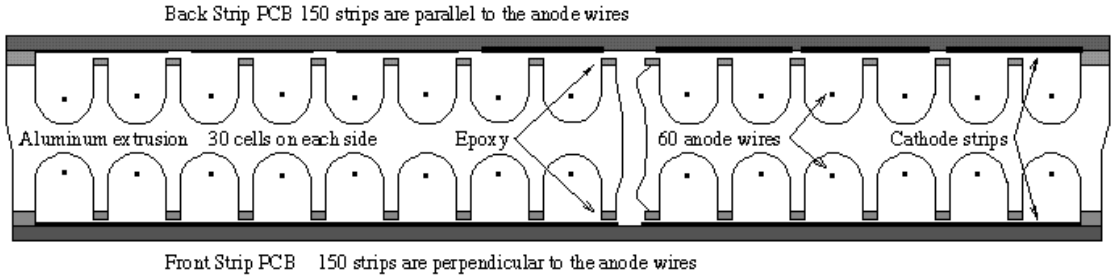

Figure III.2

Schematic diagrams of the SMD detector are given in Figures III.2 and III.3. The detector consists of a two-sided aluminum extrusion. Anode wires are strung in each channel and the cells of the extrusion are sealed by copper-clad PC boards on top and bottom. The strips come on a 2.5 mm thick copper-backed PC board. The back of this board is a continuous ground. These PC boards are glued onto the aluminum profile through three layers of epoxy with a total thickness of about 100 μm. These layers provide the electrical insulation of the strips from the aluminum profile and form a sealed gas chamber volume. A 90% Ar- 10% CO_2 gas mixture is flowed continuously through the chamber. All channels have gas flow in parallel. The pads on the top will read out the ϕ position while the bottom will read the η position. The ends of the chamber are machined to receive PC boards epoxied into place to provide wire positioning and support, high voltage distribution, and gas inlet/outlet ports.

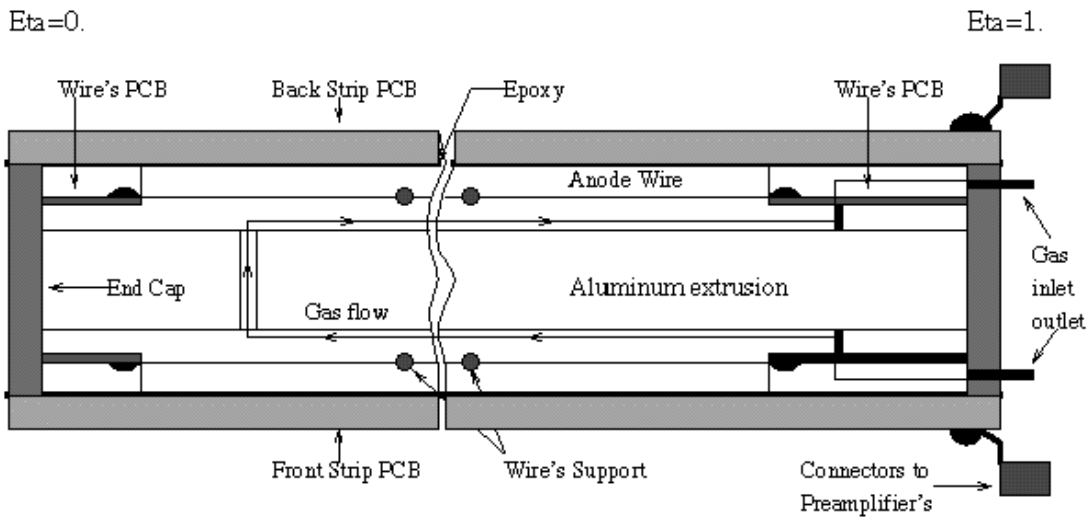

Figure III.3.

We now detail the calculations to achieve our design goal to minimize the channel-to-channel signal variation due to mechanical tolerances. We assumed that space-charge effects are negligible and that the tubes will be operated in the proportional mode. The goal of these calculations is to determine the tolerances required to produce a detector with variation of channel-to-channel performance as low as possible.

The amplification of the primary ionization signal in the proportional counter depends on the high voltage, gas density and geometrical cross section of the electrostatic surfaces. For cathodes of polygonal shape, the potential distribution can be approximated sufficiently well for our purposes as that of a coaxial structure as shown by F. Schneider (F. Schneider, EP Internal Report 78-2, CERN, Apr. 1978). The assumptions is true proportional mode, i.e., that space-charge effects are negligible. In this case, the gas amplification may be expressed as

$$\beta = \int \alpha ds, \qquad \text{(III.1)}$$

where s is the path of the ionization electron and α is the first Townsend coefficient. The integral runs between its locus of production, d, and its termination at the sense wire r_1. The nominal dimensions of the cell configuration are as follows. The diameter of the anode wire is 50 μm, the wire tension is 50 g, and the extrusion cell size is 6x6 mm^2. The gas mixture is 90%-Ar/10%-CO_2. For this gas mixture at NSTP, the charge collected on the anode wire is well represented as [A.B. Wickland, Private Communication]:

$$Q_c = 1026\, e^{(V-1500\})/78} \qquad [fC/5.9\ keV] \qquad \text{(III.2)}$$

Variation due to voltage and gas density is:

$$\beta=\beta_0 + K_1\, \Delta V/V + K_2\, \Delta\rho/\rho\ , \qquad \text{(III.3)}$$

where the parameter K_1 can be measured by a simple voltage variation (Eqn. 2), and K_2 is obtained by varying the pressure. For the calculations presented below, we used:

$K_2 = \beta_0 - K_1$.

The amplification as a function of anode wire radius:

$$\beta = \beta_0 + [\, K_2 + K_1/\ln(R/r_1)]\, \Delta r_1/r_1 \quad . \qquad \text{(III.4)}$$

Amplification due to variation of the cell radius:

$$\beta = \beta_0 - K_1/\ln(R/r_1)\, \Delta R/R \quad . \qquad \text{(III.5)}$$

Amplification for sense wire displacement from the center of symmetry:

$$\beta = \beta_0 + K_1/\ln(R/r_1)]\, (\Delta/R)^2 + (K_1 + 9\beta_0)\Delta r_1/R^2 \quad , \qquad \text{(III.6)}$$

where Δ is the wire offset due to initial positioning, gravitation or electrostatic origins. The wire offset due to gravitation is:

$$\delta_g = q\, L^2/8H \, , \qquad \text{(III.7)}$$

where q is the mass per unit length of the wire, L is the length and H is the horizontal wire tension. The wire deflection due to electrostatic forces is [S.H. Oh, W.J. Robertson, Nucl. Instr. and Meth. A309 (1991) 368]:

$$\delta_e = \pi\varepsilon_0 V^2 L^2 \delta_0/[8HR^2 \ln(R/R_1)^2 - \pi\varepsilon_0 V^2 L^2\,] \, , \qquad \text{(III.8)}$$

where δ_0 is the wire offset due to gravitation and initial wire positioning.

Using equations III.1-8 we can determine the required tolerances for the anode wire, aluminum extrusion, wire positioning and wire tension to obtain a gas gain variation less than ±10%.

Two crucial characteristics of the wires should be taken into account: variation in the wire diameter and straightness grade. The wire variation will lead to gas amplification variation according to the following table:

Diameter Tolerance	**Variation of Gas Gain**
±1%	±5.3%
±2%	±11%
±3%	±30%

Table III.2.

Experience with material for the prototype and consultation with the manufacturer [International Extrusions Inc.] has led to an adaptation of the original design for the aluminum extrusion. Achievable tolerances of ±0.006" lead to a variation in the gas gain of about ±10%.

Allowing all the error budget to the tolerances in the cell size and wire diameter, we use equations III.1-8 to calculate acceptable tolerances in the other parameters:

- Total wire displacement from the axis of symmetry due to all effects: < 265 μm
- Extrusion straightness tolerance: < 2 mm over 3 m length
- Extrusion flatness tolerance: < 1.15 mm over 1 m length
- Extrusion cell size tolerance: < ±100 μm
- Extrusion material: Aluminum alloy 6061-T6

Requirements on the chamber assembly fixtures are as follows:

- Table flatness tolerance: <1.15 mm over 1 m length
- Straightness tolerance for second datum: <200 μm at 1 m length
- Material: Aluminum alloy 6063-T5

Requirements on the wire positioning fixtures at the chamber tips and supporting lines:

- Wire positioning tolerance: < ±150 μm

Fixtures and tooling which achieve these tolerances have been built and tested for the mechanical and electrical prototypes at Wayne State University. They will be transported to UCLA for use in the first round of chamber construction in 1998. Later duplicates will be based on our experiences with these fixtures in light of performance of the completed modules.

III.2 SMD Electronics and Fabrication

III.2.1 Strip PCB Design

The design of the strip PC board satisfies the following requirements: the strip pitch of 1.42 cm (0.559") is matched to the expected transverse size of the showers. The characteristic impedance of the transmission line from strip to FEE is matched to the input impedance of the preamplifier and the lines are spaced to achieve reasonable strip-to-strip cross-capacitance, low fabrication cost and a minimum number of manufacturing steps required in the final assembly. PC Board manufacture is a 'mature' technology, which minimizes human intervention in the construction process and minimizes the overall cost.

The general design of the strip PC board (Fig. III.4) will be a plane of strips on one side and signal lines to the FEEs on the other. The characteristic impedance, Z, of these lines will depend upon the final design, but is in the neighborhood of 100 Ohms.

The propagation constant, γ, is given by

$$\gamma = [j\omega C(R + j\omega C)]^{1/2}. \qquad \text{(III.9)}$$

After propagating length l, the current I_0 will be

$$I(\omega) = I_o(\omega) \exp\{-\gamma(\omega)l\} \qquad \text{(III.10)}$$

where the real part of γ gives the attenuation in the transmission line. For high frequencies, the real part may be approximated as

$$Re[\gamma] = R/2Z \qquad \text{(III.11)}$$

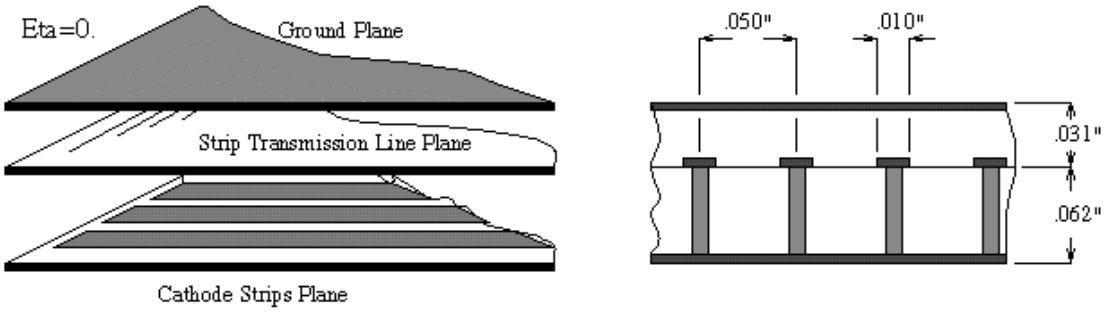

Figure III.4.

Typical line dimensions a = 100 μm, b = 500 μm and ρ = 1.7 10^{-8} Ω-m give an attenuation constant α= 0.0034/m. Thus, we expect a signal attenuation of about 1% for the signals which propagate from the region near η=0 to the FEE cards located near η=1. The maximum delay time for these same signals is about 20 ns. The overall capacitances of the strip plus delay line is given in the following table:

	η = 0	η= 0.5	η=1.0
η-Strips	285 pF	260/347 pF	333 pF
ϕ-Strips	244 pF		246 pF

Table III.3.

As noted in the first section, there is a jump in the width of the strips at η = 0.5.

III.2.2 Preamplifiers and Readout

III.2.2.1 Design Parameters

The design of the readout electronics was made to satisfy the physics requirements, mechanical consideration, and integration of the SMD into the EMC and STAR. The reliability, accessibility, and possibility to make future upgrades also were considered. The physics requirements (see section VII.2.b for details), lead to overall dynamic range 1:640. The smallest signal from MIP need to be detected is around 4fC (at HV = 1380 V). The capacitance of the readout strip in average 260 pF and vary depending on the strip position vs. eta (strip length is projective) and also on the length of the strip transmission line to the front-end motherboard. The total collection time for ions in SMD gas mixture is around 30 ns, so that ion tale cancellation is desired (see details in section VII.2.b). Power consumption is need to be at lowest possible level (30-40 W power dissipation or each SMD module is acceptable) to simplify the integration. High integrity of the readout electronics is preferable to avoid the long transportation of the analog signal in noisy environment. The test run experience with the small prototypes shows that appropriate gain for the preamplifier/shaper need to be close to 20 mV/fC. The noise at level ENC 6000 electrons for strip capacitance around 300 pF is acceptable. This level of noise will allow to operate SMD at high voltage close to 1380 V to detect MIP with reasonable efficiency and to avoid the problems with gas saturation (space charge effect near the anode wire) for up to 30 GeV electromagnetic showers. The crosstalk as measured for the full scale chamber electrical pre-prototype is around 3% (the worst case for the strips located at eta=0 end of the module) due to cross capacitance of the strip transmission lines. The crosstalk for the preamplifier/shaper at level 1% is acceptable. The precision of the internal calibration of the

channels of preamplifier/shaper is need to be no worse than +/- 7%, so the overall calibration of the channels of the SMD will be known with accuracy +/- 10% prior data taking.

III.2.3 Preamplifier Mechanical Integration

From a mechanical integration viewpoint, there are several reasons to put the SMD FEE at one end of the EMC module as opposed to a solution which embeds the electronics within the module:

- Operational: The experience with these types of chambers proves that reliability of the FEE is much lower than the reliability of the chamber itself.
- Preamps at this moment are in the prototype stage. To install a few modules on 'Day One' we need to separate the mechanics and electronics of the SMD.
- Simplification of the SMD integration into the EMC. (We avoid the problem of interference between the SMD cables and EMC fibers on the sides of the EMC module.)
- Simplification of the EMC integration into STAR. (Again, problems related to fiber and cable routing through the same channels, as well as the new design of the EMC optical connectors.)

Access to the preamps during RHIC operation. Repairs, upgrades, etc., can be made without disassembling the EMC or even removing the modules from the barrel.

III.2.3.1 Envelope

Placement of the FEEs on the end of the modules has a slight ramification on the physics because the gap between the barrel and the endcap must be increased to 38 mm to allow enough room for the SMD preamps. Recent simulations by Akio Ogawa (Penn. State) shows that there are no significant losses in acceptance for this configuration, at least for p-p physics at RHIC.

III.2.3.2 Interface

For each SMD module, there are 300 channels of strips to be read out. The preamplifiers will be on the Mother Board at the eta=1 end of the module. The dimensions available for the MB are a trapezoid with a top side of 210 mm, a base of 230 mm and a height of 308 mm. (677 cm^2).

All interfaces for the SMD system are located on the top of the EMC module on the η=1 side in order to simplify the procedure for the installation of the EMC into STAR.

An IDC ribbon cable (Thomas-Betts, Type 20067) of length 3-5 cm will be soldered to the Strip PCB at the η = 1 end of the chamber. (Thomas-Betts, Type 609) Connectors will be used to connect the Mother Boards to the chambers. The pre-amp cooling tubes will be cooled by compressed air through 1/4" OD Poly-Flo tubing (44-P-1/4, Imperial Eastman).

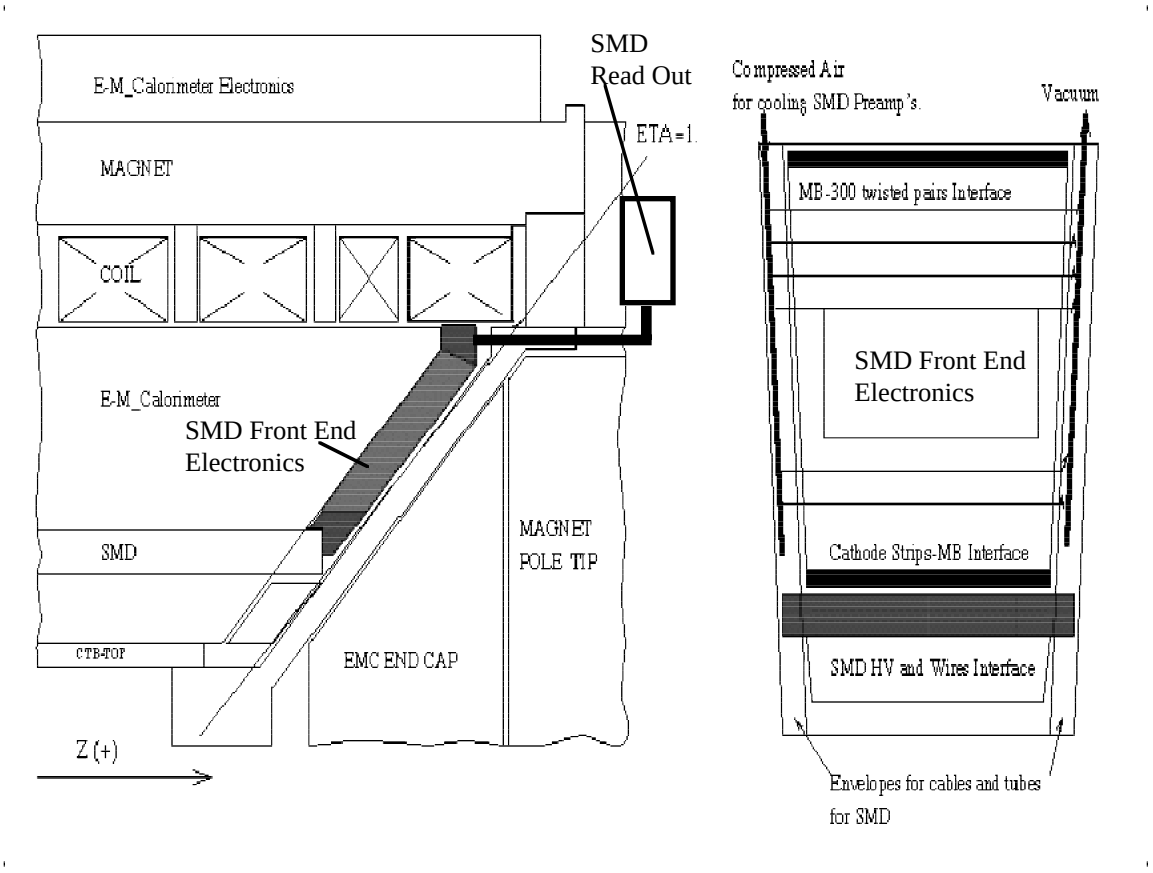

Figure III.8.

III.2.3.3 Cooling System

The total power dissipation in the volume of the electronics at the eta=1 end of the each EMC module is expected to be < 30 W. Using a mechanical 'pre-prototype' we have developed an empirical formula for the temperature of the boards as a function of air flow rate : T=66 - Q/10,
where T(C) and Q (cf/h). The temperature of the input air was 25 C. To allow a safety factor of three, we will specify a cooling flow of 12 cubic feet per minute, again assuming the ambient air temperature is 25 C. The air temperature rise in this case was expected to be 4 C. Pre-cooled air would lead to problems with condensation.

III.3 Prototype Performance Studies

III.3.1 Introduction

The performance of the SMD candidate designs were studied over the period from 1992-1997 at the IHEP U-70 accelerator (Protvino, Russia) and at the BNL-AGS. Below, we present the performance of the baseline gaseous prototype designs in the wire/strip and strip/strip configurations only. Complete information about these studies can be found in

- B. Chuiko et al, IHEP Preprint 92-104, Protvino, 1992 First SciFI SMD Prototype

- S. Alimenko et al, Nucl. Instr. and Meth. A365 (1995) 92. The Last SciFI SMD Prototypes
- V. Belousov et al., Nucl. Instr. and Meth. A369 (1996) 45. PST SMD Prototype.
- S. Alimenko et al., Prib. Tekh. Eksp. 1997, N3 39. The Last Gaseous SMD in Wire/Strip Configuration.
- S. Bennett et al., Star Note (in preparation). The Small Gaseous SMD Prototype in the Strip/Strip Configuration, Final Design, Test '97.

The latest strip/strip small SMD prototype in the final design configuration was constructed and tested in 1997. This photograph (Figure III.9) shows the SMD prototypes under construction.

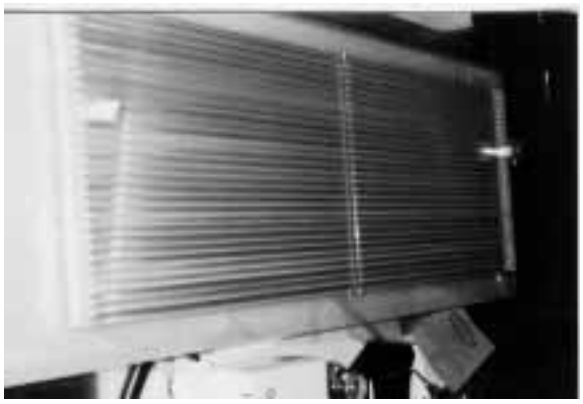

Figure III.9

Figure III.10 shows the assembled small prototype being bench-tested prior to installation into the small EMC prototype.

The detector construction was similar to the procedure described in section III.1.3, with cell size close to the final design and strip dimensions given in Table III.1 The gas mixture used in the prototype test was 90% Ar- 10% CO_2. The extrusion used for the prototype was rectangular in cross section with 32 cells of size 222 mm x 685 mm x 24 mm. The readout consisted of 32 x 32 channels of strips. The pulses from each strip were amplified by a two-stage device based on a 'Garantija' current amplifier and digitized by 11-bit LeCroy 4300 ADCs with a sensitivity of 0.25 pC/count and a 400 ns gate.

III.3.2 Chamber Gain

The optimal value of the wire/strip

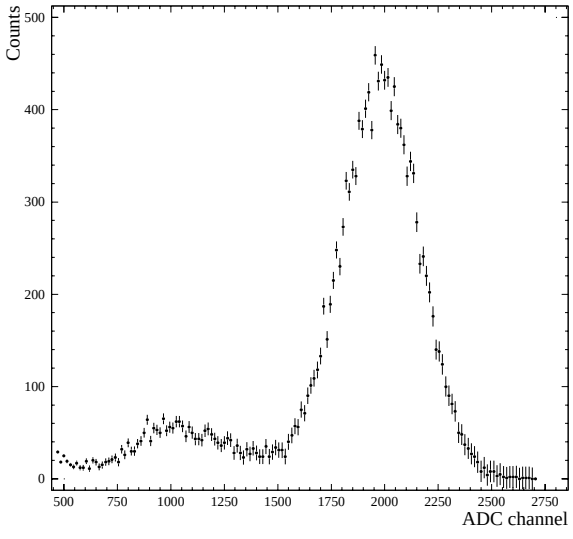

Figure III.11

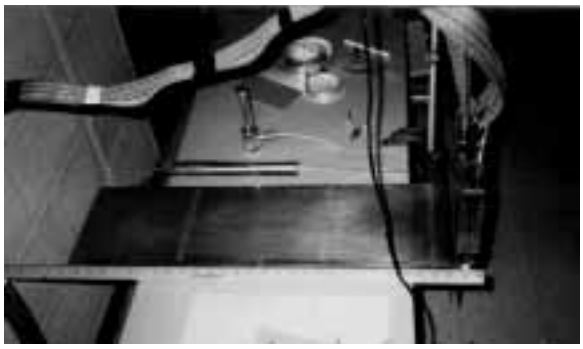

Figure III.10

SMD gas gain is constrained by space charge effects on the one hand and by signal-to-noise considerations on the other. Another important consideration is the reliability of the chamber over long periods. For this reason, it is important to determine the characteristics of the SMD at the lowest possible gas gain. Our goal is to operate

the chamber in the proportional mode. Up to 30 GeV, it is desirable to eliminate problems of signal saturation due to space charge effects. It is important to minimize the systematic uncertainties in the measurement of direct photons with the SMD.

Before placement in the test beam, the chamber was irradiated with ^{55}FE X-rays to determine the appropriate gas gain. A typical pulse height spectrum is given in Figure III.11.

The ratio of the pulse heights for photons of energy 3 and 5.9 keV for the Fe source indicates that the chamber is operating in the proportional mode. A gain drop was observed when the density of the positive ions along the wire exceeded a critical value equal to 7 x 10^6 per mm. The optimal value for the applied high voltage in the test beam was constrained
by signal-to-noise considerations. The high voltage was set to 1500 V for test beam in the energy range 0.1-0.7 GeV; corresponding to a gas gain of about 10^4. Between 13.3 and 26.6 GeV, the voltage was set to 1450 V, corresponding to a gas gain of 3-5 x 10^3. Under these conditions, Monte-Carlo calculations indicate that the maximum density of positive ions along the wire (in the region of the SMD near the shower axis) was 3 x 10^6 /mm; which does not exceed the critical value.

III.3.3 Chamber Response and Energy Resolution

The response of the front and back planes of the SMD for electromagnetic showers is given in the following Figure III.12.

In the energy range from 0.5 to 5 GeV, at a depth of 5X0 inside the EMC, the SMD has an approximately linear response versus energy. The ionization at the back plane of the SMD is about 10% lower than the front plane. The energy resolution in the front plane is given approximately by

$$\sigma / E = 12\% + 86\% / \sqrt{E}\ [\text{GeV}]. \qquad \text{(III.13)}$$

The energy resolution in the back plane is 3-4% worse than the front plane. The difference in behavior between the front and back was observed for the first time in previous studies of the SciFI variant of the SMD (S. Alimenko et al, Nucl. Inst. and Meth. A365 (1995) 92). The detector response depends on the material inserted in front of the SMD. The presence of low-Z material in front of the detector leads to a partial cutoff and transverse broadening of the soft component of the electromagnetic shower due to multiple scatter in this material. This leads in turn to a signal drop in the detector, as well as a degradation of the spatial and energy resolutions. From this point of view the optimal sequence of the tiles in the EMC would point to a Pb tile just in front of the SMD.

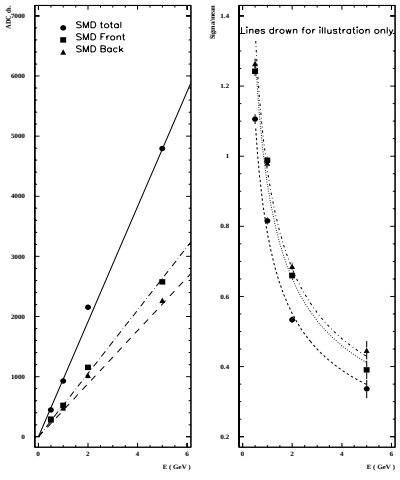

Figure III.12.

III.3.4 Transverse Shower Profiles

As pointed out above, the shower position resolution, multishower resolving power, and electron-hadron separation provided by the SMD relies on the analysis of the transverse shower profile. A precise measurement of the shower shape is important for the tuning of Monte-Carlo programs and as input for future data analysis. Fig III.13a shows the normalized energy deposition in the SMD for showers for electrons from 1 to 26.6 GeV. The SMD is located 5 X_o inside the EMC. Fig. III.13b gives the shower profile for 26.6 GeV electrons at SMD positions at 3X0 and 7X0 inside the EMC.

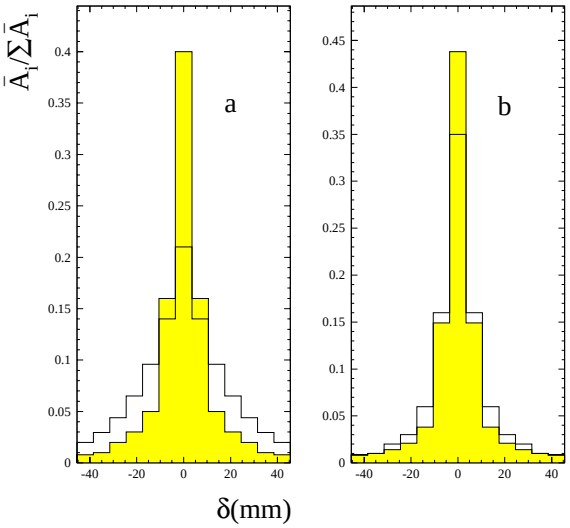

Figure III.13.

It is common to approximate the shower shape as the sum of two exponentials:

$$dE/dx = a_1 e^{-x/b1} + a_2 e^{-x/b2} . \quad \text{(III.14)}$$

This expression is convenient to compare our results with the CDF beam results. As with the CDF results, the shower shape is constant about 7 GeV. Both sets of results show that in this energy range the shower shape is well described with the values b_1 = 0.5 cm and b_2 = 2.3 cm. for the wire plane and b_1 = 0.6 cm and b_2 = 2.8 cm for the strip plane. We should point out, however, that this approximation only seems to hold near the shower axis. In future analysis we use a lateral shower density which is the sum of three exponentials whose contributions are noted as A,B, and C. Fig. III.14 shows the mean energy deposited in the SMC vs. the distance from the shower axis. The data points are the results from the test run for 26.6 GeV electrons with the detector positioned at 7 X_0 inside the EMC. The solid curve through the data is a fit to the experimental data (χ^2/ndf = 1.18) using the sum of three exponentials. The relative contributions are given by the dashed lines.

The experimental results show that the parameters in the exponentials vary only weakly with position inside the EMC (from 3X0 to 7X0). Their values are 0.35 cm, 0.9 cm and 12.0 cm respectively. In the table below we present the results of the shower shape analysis for the three positions of the SMD inside the EMC.

SMD Position	**Percent Contribution**		
	A	B	C
3X0	48.2	33.2	18.6
5X0	37.0	47.3	15.7
7X0	24.3	59.8	15.9

Table III.6

These results show that 90% of the energy is deposited within 3.5 cm of the shower axis. When the position of the SMD inside the EMC is changed, there is a redistribution of the contributions A and B to the energy profile. At the same time, 90% of all the energy deposition for the SciFi SMD was deposited within a distance of about 1.5 cm from the shower axis. We believe this difference comes from the transverse development of the soft components of the electromagnetic shower and depends strongly on the particular detector materials.

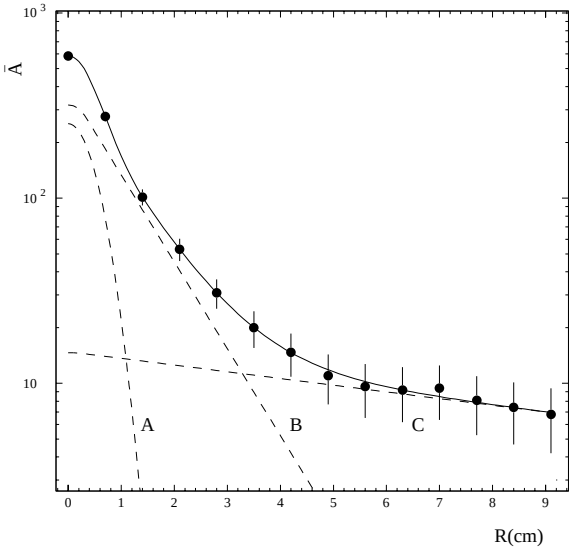

Figure III.14.

III.3.5 Position Resolution

The position resolution was studied as a function of energy and SMD position. All measurements were made for an impact point at the center of a strip or wire channel. Two methods were used to determine the shower axis (Y_s) in the plane of the SMD:

$$Y_s = \Sigma_i w_i y_i / \Sigma_i w_i , \qquad \text{(III.15)}$$

where y_i is the geometrical center of the i-th element and W_i is the energy deposition E_i in the i-th element for the simple center-of-gravity method. For the ''logarithmic' algorithm proposed by T.C. Awes et al (T.C. Awes et al., Nucl. Instr. and Meth. A311 (1992) 130), w_i is a weight for the i-th element determined as follows:

$$w_i = \max[\, 0, W + \ln(E_i / \Sigma_i E_i) \,] \qquad \text{(III.16)}$$

where W is a constant determined empirically. The use of the logarithm this expression is motivated by the exponential falloff of the shower profile. This corrects the deficient behavior of the linear weight approach where a centrally hit element will contain most of the energy and will systematically pull the position calculation. The choice of W determines the relative importance of the energy deposition in the tails and provides a natural threshold. For example, for W=2, all the strips with an energy deposit of less than 13.5% of the total energy will not be considered.

Fig III.15 shows the systematic pull in the position calculation in the case of a linear weight. This is the experimental result from the 1997 test with 5 GeV electromagnetic showers. The uniform distribution of the impact parameter across the strip surface in the case of linear weighting in the expression for the center of gravity leads to a systematic shift to the geometrical center of the strip (in the region ± 2.5 mm from the center of the strip). The logarithmic method appears to be free of this problem. This picture represents data from the front and back planes and is averaged over the entire SMD.

The spatial resolution data for the SMD were determined from shower profiles for four energies in the 1997 beam test. These results are given in the following table. The first column in the table gives the distance from the beam axis in mm. In the next columns are the relative energy deposited in percent. The integral over the shower profile at a given energy is 100%.

Dist [mm]	E = 0.5 GeV [%]	E = 1. 0 GeV [%]	E = 2.0 GeV [%]	E = 5.0 GeV [%]
0-5	29.5 ± 0.9	35.7 ± 0.8	39.2 ± 0.5	42.3 ± 0.5
5-10	22.3 ± 0.8	24.8 ± 0.6	25.4 ± 0.5	25.6 ± 0.4
10-15	18.5 ± 0.8	17.2 ± 0.5	17.2 ± 0.4	15.8 ± 0.4
15-20	10.0 ± 0.5	8.2 ± 0.3	6.9 ± 0.3	6.9 ± 0.3
20-25	5.9 ± 0.4	4.2 ± 0.2	3.4 ± 0.2	3.5 ± 0.2
25-30	4.7 ± 0.4	3.3 ± 0.2	2.7 ± 0.2	2.3 ± 0.1
30-35	3.1 ± 0.3	2.3 ± 0.2	1.9 ± 0.2	1.5 ± 0.1
35-40	2.3 ± 0.3	1.9 ± 0.2	1.2 ± 0.1	0.9 ± 0.1

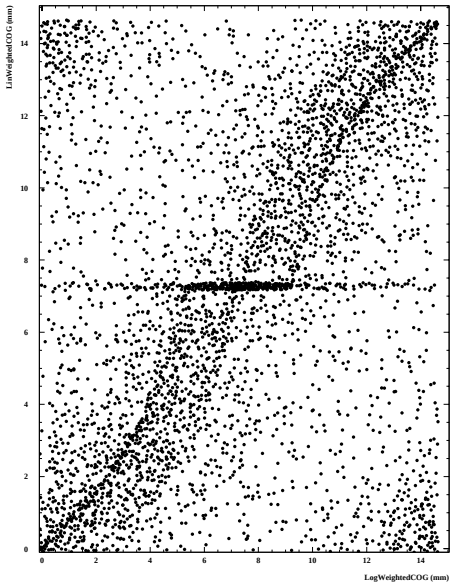

Figure III.15.

40-45	1.9 ± 0.3	1.3 ± 0.1	1.0 ± 0.1	0.8 ± 0.1
45-50	1.9 ± 0.3	1.0 ± 0.1	0.8 ± 0.1	0.5 ± 0.06

Table III.7

Dependence of the shower width on energy is presented in fig. III.16. The shower width gets narrower is the energy increases.

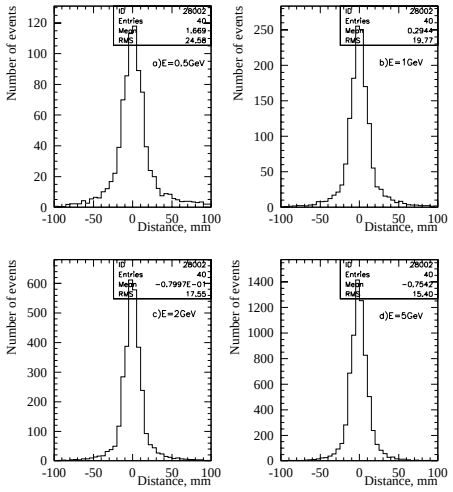

Figure III.16.

Figure III.17 shows the position resolution in the front and back planes of the SMD for the 1997 Test. The resolution in the front and back planes go like

σ_{front} [mm] = 2.4 mm + 5.6 mm / $\sqrt{E}$ [GeV] , and
σ_{back} [mm] = 3.2 mm + 5.8 mm / $\sqrt{E}$ [GeV] .

The parameter W=2 was taken to calculate the center of gravity of the electromagnetic shower.

We give a comparison between GEANT simulations of the shower profiles and data for four test beam energies in fig. III.18.

The GEANT shower profile is narrower than the experimental one in the energy range from 0.5 to 5 GeV. The central value of the deposited energy in the GEANT calculation is also higher than experiment by about 20-40%, depending on energy. In the tails of the distribution, the experimental data is higher by a factor of 1.5 to 2.5. The GEANT profile agrees more closely with experiment as the energy increases (see fig. III.19)

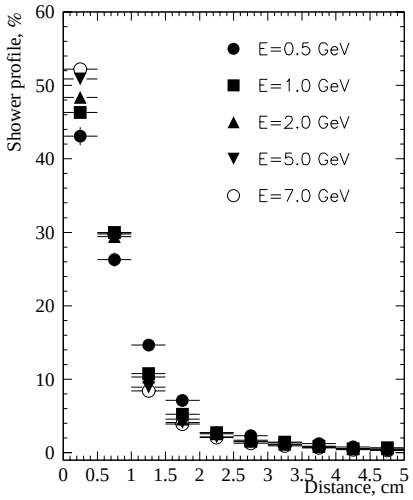

Figure III.18

III.3.5 Electron-Hadron Rejection

To compare the electron/hadron rejection power for the longitudinally segmented EMC (5X0 + 20X0), a non-segmented EMC (25X0) and a non-segmented EMC with an SMD (25X0 + SMD), these detectors were tested with beams of π^- at 39 GeV and e^- at 26.6 GeV. The rejection coefficient K was defined as the probability to identify a hadron as an electron for 90% electron detection efficiency. The 25X0 EMC provided a rejection level of $K = 1.8\ 10^{-2}$. The longitudinal segmentation improved the rejection by a factor of about 6 for $K = 3 \times 10^{-3}$. The information about the energy deposition in the 25X0 EMC and the SMD gave $K = 5.1\ 10^{-3}$. Additional information about the shower width in the SMD slightly improved the rejection, due to correlations between the SMD energy deposition and the shower width. Therefore, the above results show that the SMD improves the hadron rejection power by a factor of 3.5 as compared to the rejection of a non-segmented EMC. It is poorer by 1.7 times compared to a longitudinally segmented EMC.

One of the advantages of the final double-sided design of the SMD is the independent measurement of the primary ionization in two gas samples inside the EMC. Large fluctuations on the ionization in thin gas layers can cause the ionization from a single minimum ionizing particle to be comparable to that of an electromagnetic shower of a few GeV. This leads to a degradation of the SMD electron/hadron rejection power. In the case of two independent gas samples, the probability of such an event is obviously smaller.

A few methods of electron/hadron separation were investigated. The main problem for the SMD is the absence of an energy-independent variable to be used for e/h rejection. Below approximately 10 GeV, the ratio of SMD/EMC signals for electrons is a constant. But as the energy increases, the position of the shower maximum shifts logarithmically and the above ratio decreases. Above about 10 GeV the so-called weighted radius for the

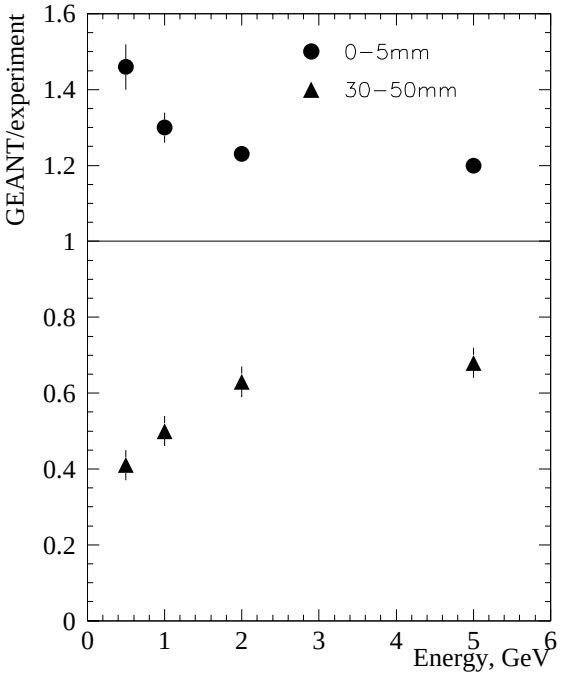

Figure III.19

electromagnetic shower is independent of energy. This follows from the invariance of the transverse shape of the shower as noted above.

Here we show one of the approaches to achieve e/h separation. First, separate cuts on energy deposition are made for the front and back planes: the surviving electrons have 90% detection efficiency. Fig. III.20(a) gives the entire data sample for electrons and hadrons (Run 53, Test 1997, 5 GeV) as well as the cuts applied to identify electrons.

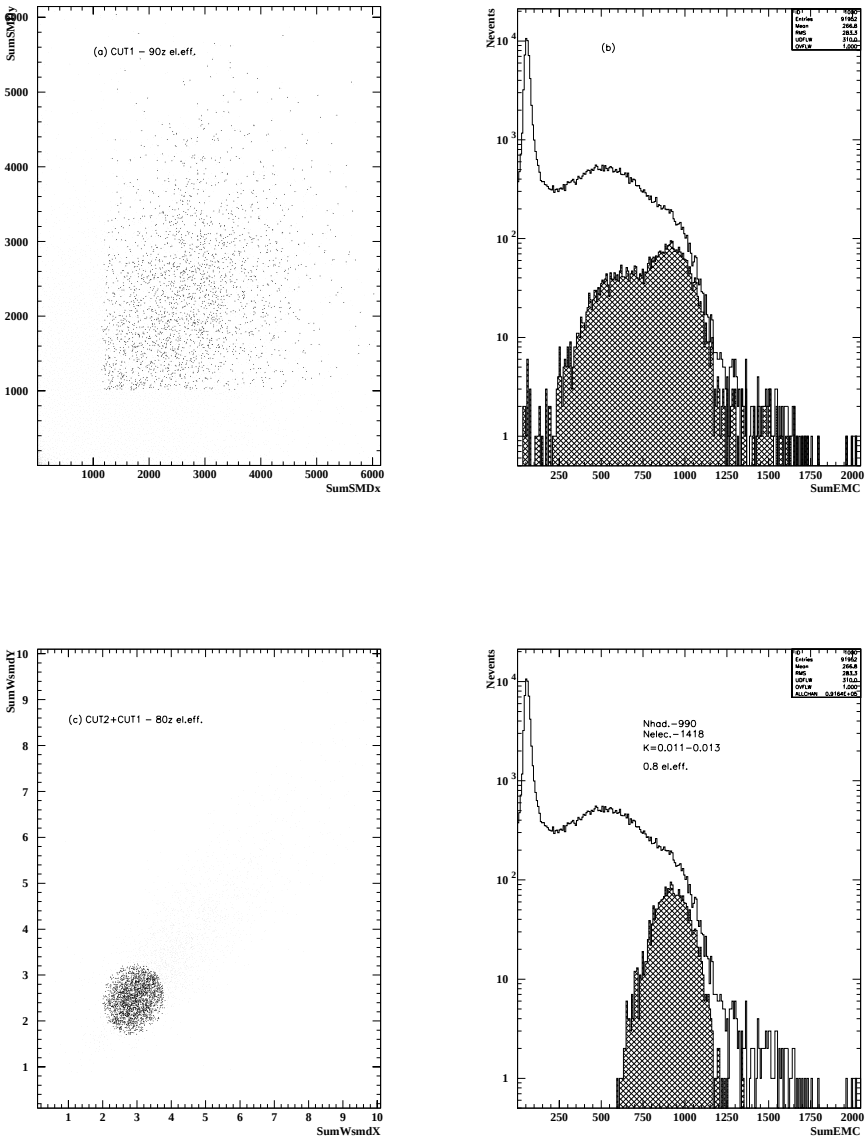

Figure 111.20

This figure also illustrates the independence of the ionization in front and back planes of the SMD in case of hadrons. Fig III.20(b) shows the amplitude spectra in the

EMC for the entire data sample and surviving events after applying cuts in the SMD. The rejection power of SMD itself comparable to rejection power of the non-segmented EMC, and is close to 30:1 for this particular energy, with an electron efficiency of 80%.

As it can be clearly seen from this figure, the SMD reject events different from those rejected by applying single cut on the EMC (for events with small amplitudes in the calorimeter). This allows us to increase the rejection power of the combined detector (EMC/SMD) by applying cuts which take into account information and from the EMC also. Fig III.20(c) shows the distribution of the ratio of the sum of the strips logarithmic weights over energy deposition in the EMC for the front vs. back planes of the SMD for the surviving the first cuts. The electrons events are mostly located in the 'head' of the 'comet', while the hadrons events are in the halo. In this figure, the marked area in the 'head of comet' contains 80% of the all electrons from the original data sample. Fig III.20(d) shows the amplitude spectra in the EMC for the surviving events. The hatched distribution is the amplitude of the surviving hadrons. The overall rejection power for the detector is 0.012±0.001 for 80% electron efficiency. In the energy range from 0.5 to 5 GeV the information from SMD improved the rejection power of the non-segmented EMC about a factor of 3.

III.3.6 π^0/γ Separation

A study has been carried out to investigate the use of the SMD to separate showers coming from single photons from those arising from neutral pin decay. All results were obtained for $\eta = 0$ for the STAR geometry. Two parameters of the shower energy deposition in the SMD are defined below: the energy-weighted-radius, R and the 'inertial moment', ER^2 of the shower. The coefficient of rejection is defined for 80% single gamma detection. For each shower, these parameters are calculated separately for each of the two SMD planes.

The shower center of gravity was calculated as:

$$X_c = \Sigma w_i x_i / \Sigma w_i \quad , \qquad \text{(III.17)}$$

where w_i and x_i are respectively the logarithmic weight and the coordinate of each element. The energy weighted parameters $R_{x,y}$ were calculated as:

$$< R_x > = [\ \Sigma w_i (x_i - x_c)^2 \ / \Sigma w_i \ ]^{1/2} \quad . \qquad \text{(III.18)}$$

The mean weighted radius, R was defined as

$$R = (R_x^2 + R_y^2)^{1/2} \qquad \text{(III.19)}$$

The second parameter, ER^2 , which provides information about the longitudinal shower development, was first calculated for each layer and summed in quadrature as above.
On the scatter-plot of ER^2 vs. R we have marked off the area containing 80% of the single γ showers and consider showers within this area to be 'single γ' while all showers outside this area are classified as neutral pin showers. Using this definition, we determined the π^0 probability separation for 80% single γ detection as a function of incident shower energy. Fig. III.21 gives the results of this study.

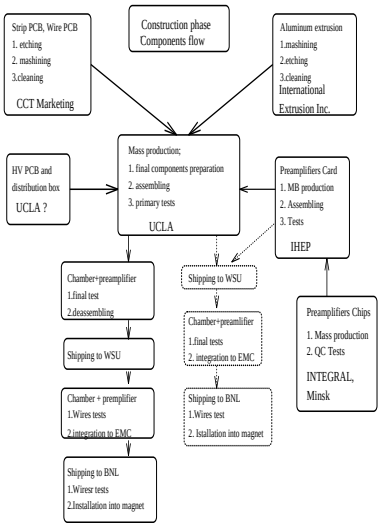

Figure 1 III.21.

The energy region from 3 to 7 GeV is important in the QGP search by measuring single photons. From this point of view, it is preferable to locate the SMD as the 5X0 position inside the EMC.

The study of these parameters defined above shows that a shower initiated by photons and neutral pions can be distinguished mainly by use of the quantity R. The use of the inertial moment parameter resulted in negligible improvement, mainly due to the poor energy resolution of the SMD.

III.4 Detector Assembly, Tests and Quality Controls

The detectors will be assembled in a production facility to be set up at UCLA. This facility will be located in the Science and Technology Research Building (STRB) which will be available for beneficial occupancy in April, 1998. The physical plant available for STAR will be cost-shared with another group building muon chambers, resulting in a considerable cost savings. The SMD group has been allocated approximately 1500 sq. ft of open floor space for preparation and staging work. Assembly of the modules will be performed in a 1500 sq. ft clean room. Approximately 1000 sq. ft of additional laboratory space in Knudsen Hall can be committed for such purposes as chamber tests or temporary staging work. Finally, the UCLA machine shop is available for support work on a scale consistent with the planned module production schedule.

The total number of modules to be produced is 120 plus some spares which will be decided at a later date.

Economic considerations require us to purchase and store a large fraction of the raw materials for the SMD modules. It is anticipated that the space available in the STRB will be adequate for storage of these materials. During staging of many modules, we may utilize the additional storage or work space in Knudsen Hall.

In the staging for the first 15 modules, we will divide the production procedures approximately as follows: cleaning, light machining and temporary storage will be confined to the main assembly area. After preparation, the pieces will be examined for quality assurance on special test beds and vacuum tables in the clean room.

The modules are assembled by first applying a uniform layer of about 100 μm of epoxy to the extrusion edges and allowing it to dry. This serves to electrically insulate the extrusion from the copper of the readout pads. This step is performed first to avoid contamination of the anode wires by stray droplets of epoxy. Next, the wire PC boards, anode wire nylon support lines and elements of the chamber tips are epoxied in place. The anode wires are strung, then soldered in place. The wire stringing procedure will be checked by means of an automated system which determines the location and tension of each wire by means of a laser diode and photosensor (a bar code reader). The wire is gently set into os-

cillation by means of an air current and the resultant frequency of vibration noted using the Fourier transform of the sensor signal measured on a digital oscilloscope. This method worked very well for the STAR TPC sector construction.

The wires are then glued in position to the nylon support lines to prevent sagging under gravity under any orientation. The gas volume is then sealed by gluing the pad PC board in place. This assembly is then flipped over and the procedure repeated for the other side of the extrusion.

Assembly procedures will incorporate certain quality assurance checks such as measurement of wire tension, gas flow rate/ hermiticity and high voltage breakdown. Finally, the completed modules will be tested in Knudsen Hall for signal uniformity using anode wire pulsing, radioactive sources and/or cosmic rays.

The assembly procedures are as follows:

General Area:

1) Cleansing of extrusion/preliminary inspection
2) Cleansing of PC boards/preliminary inspection

Clean Room:

1) Inspection of extrusion for defects, straightness, flatness
2) Covering extrusion edges by epoxy
3) Gluing of Wire PCs, Wire Support Lines, Chamber Tips
4) Stringing/Soldering of Anode Wires
5) Check of Wire Tension
6) Gluing of Wires to Support Lines
7) Gluing of Strip PC Boards
8) Check for Electrical Isolation/Short Circuits.
9) Reverse Extrusion and Repeat (1-9) for Other Side.
10) Final Chamber Tip Assembly

Testing:

1) Gas Flow/Pressure Drops/Hermiticity
2) Electrical Isolation/Short Circuit Check
3) High Voltage Breakdown Check
4) Pulsing Check for Pad Response
5) Radioactive Source Check

Vendors for the components critical for SMD mass production have now been identified. Figure III.22 gives the overall 'components flow' scenario and major stages of the components preparation.

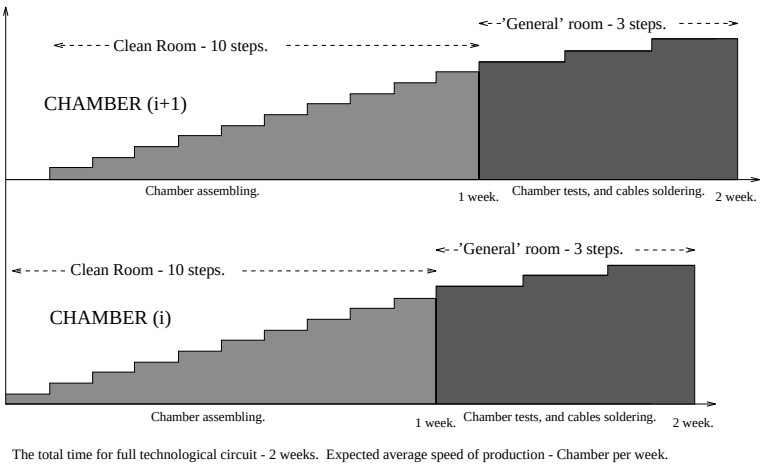

Figure III.22

At the present time, the first set of aluminum extrusions and strip PCBs produced by International Extrusion and CCT have been received. A portion of the assembly fixtures have been made for the construction of the full-scale mechanical prototype and full-scale operational chamber. The full-scale SMD mechanical prototype was constructed to be incorporated into the full-scale EMC mechanical prototype, as well as to test the assembly equipment and assembly protocols. Both the extrusion and strip PCBs passed out quality control tests and satisfy the design requirements. The deviation of the dimensions from the nominal values are in the acceptable range. Fig. III.23 shows the measured flatness of the full-scale SMD mechanical prototype after assembly using a 'vacuum gluing' table.

The conclusion of this study is that the mechanical parameters of the SMD will not lead to any problems related to integration of the SMD into the EMC modules. Our present construction methods will allow us to mass produce SMD modules of the required quality.

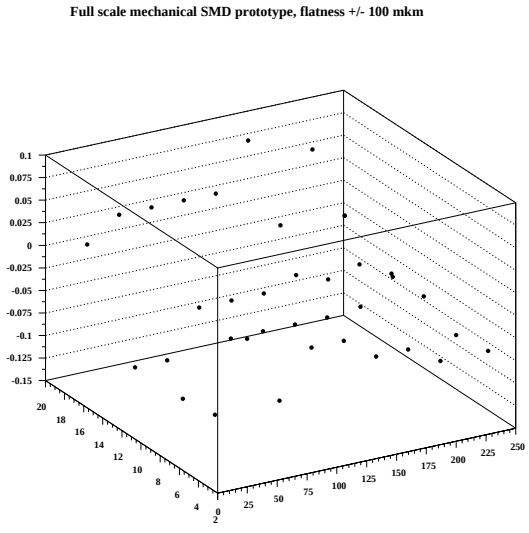

Figure III.23